We are IntechOpen, the world's leading publisher of Open Access books Built by scientists, for scientists

6,900
Open access books available

185,000
International authors and editors

200M
Downloads

Our authors are among the

154
Countries delivered to

TOP 1%
most cited scientists

12.2%
Contributors from top 500 universities



WEB OF SCIENCE™

Selection of our books indexed in the Book Citation Index in Web of Science™ Core Collection (BKCI)

Interested in publishing with us?
Contact book.department@intechopen.com

Numbers displayed above are based on latest data collected.
For more information visit www.intechopen.com



3

Elaboration of a Specific Class of Metamaterial: Glass in Single Crystal

Bertrand Poumellec, Matthieu Lancry, Santhi Ani-Joseph,
Guy Dhalenne and Romuald Saint Martin
Institut de Chimie Moléculaire et des Matériaux d'Orsay,
Université de Paris Sud 11, Orsay,
France

1. Introduction

Metamaterials are composite materials, which can exhibit some interesting optical properties, which is usually not found in natural materials. Some examples of the properties that can be obtained and controlled in these materials are negative refraction and artificial magnetism [1, 2]. The wave vector k of a wave propagating through such a left-handed substance is anti-parallel to its Poynting-vector S. This remarkable property has far-reaching consequences. Usually these materials have some periodic or quasi-periodic structure. Such photonic metacrystals are composed of periodic assembly of dielectric or metallo-dielectric structures that are designed to affect the propagation of electromagnetic waves. In particular, they should have refraction indices significantly different. The assembly can be unidimensional as in periodic multilayered materials, or two-dimensional with periodically spaced rods or fibers aligned in arrays, or 3D like silica spheres in Opal.

When the characteristic length scale of constituting elements is much smaller than the radiation wavelength, they are called photonic crystals (PC). This is because these structures avoid diffraction. The electromagnetic wave passing through the PC will feel only the effective parameters of the material such as the effective magnetic permeability, effective permittivity, etc. They therefore can in good approximation be considered as continuous media with some effective electrodynamic properties. For these reasons, metamaterials do not necessarily possess a photonic band gap (PBG), which is a striking difference compared to PCs. Nevertheless it is interesting to look for the possibilities of opening up a PBG, for extensive applications and also for better insight into the optical properties of the material [3, 4].

There are various methods to fabricate ordered composites like metamaterials. They are collected, for instance, in the book Nanophotonics by Prasad [5] or in Chemistry of Nanomaterials by Rao et al.[1]. They are classified into two categories, those, which are carried out by engineering, and those, which are obtained by self-organization. In the former category, there are various techniques including nanolithography, the deposit of the multi-layer films (CVD, Langmuir-Blodget) etc. The most commonly practiced method for preparing these materials are largely based on lithography, which uses a pre-fabricated photo mask as a master from which the final pattern is derived. Self-organization is an

unconventional way of manufacturing photonic crystals by purely chemical method and it would open up new fields of application avoiding the problems related to engraving. Especially, in self organization, no one has described a way of synthesis starting from high temperatures, although it has some advantages like low cost, large volume and weak OH content (absorbing in the near-IR range). This last advantage can be made profitable to obtain materials compatible with the existing optical fiber networks.

In the past, researchers [6-12] showed the possibility of obtaining such ordered structures starting from eutectic compositions. Eutectics correspond to particular points in the phase diagram between the liquid phase and a solid phase, the composition of the liquid is fixed but it decomposes into two solid phases of different compositions, on cooling. A microstructure appears, but very often it is disordered. Nevertheless for some sets of elaboration parameters, ordered microstructures settle. Those can be defined by the kinetics of the growing environment, speed of cooling and also by some intrinsic parameters like diffusion, chemical kinetics of phase formation etc.

In this paper, we report the use of this method for synthesizing a new category of composites: equidistant glass fibers in a single crystal matrix. This is carried out at high temperature, by a technique called 'floating zone'/'melting zone' associated with an image furnace [7, 10]. The apparatus is described in Figure 1. A floating zone is established between a single crystal (the seed) and a polycrystalline rod (the feed rod) by using the radiative heat provided by two halogen lamps in an image furnace. These ways of development are essentially adapted to the development of large volume of single crystal (see Fig. 1).

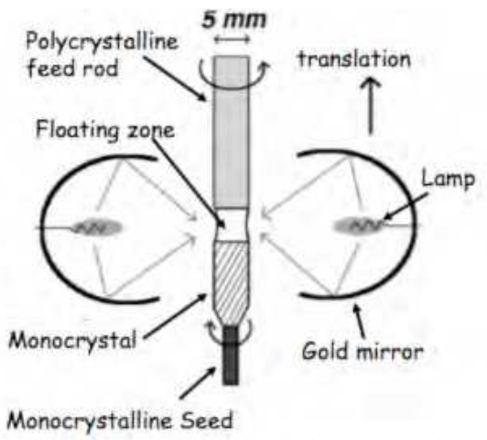


Fig. 1. Scheme of the floating zone apparatus using a double image furnace.

2. Synthesis route

The system that we investigated is $CuO\text{-}SiO_2\text{-}GeO_2$ around the composition $CuGe_xSi_yO_{1+2(x+y)}$ with $1 \leq x+y \leq 1.4$ and $0 \leq y/x \leq 0.4$. $CuGeO_3$ is an inorganic crystal that was studied in our laboratory for other properties [6, 10]. This crystal is orthorhombic with a space group Pbmm and the crystalline parameters: a = 4.79Å, b = 8.49 Å, c = 2.94 Å. It can dissolve Ni/Mn on its network of octahedral Cu and Si on its tetrahedral Ge network. Even though it can dissolve Si into its atomic tetrahedral chain, there is a limit (typ.: a fraction of a few %) in the atomic fraction of Si which can thus replace Ge, beyond which it will not produce a single phase on solidification. We discovered this while looking for methods to

obtain a self-organized composite. Moreover, as we increase the atomic fraction of Si in the starting composition, the nature and quality of the crystal varies. In fact, we could not confirm if we really have a eutectic or not in our case. This is because, a detailed chemical analysis by the electron microprobe method [6], both on the crystalline matrix and on the fibers, confirmed the presence of Si at these two locations. If it were a eutectic, more chances would be that Si would not replace Ge in the crystalline matrix, instead stand alone as silica fibers.

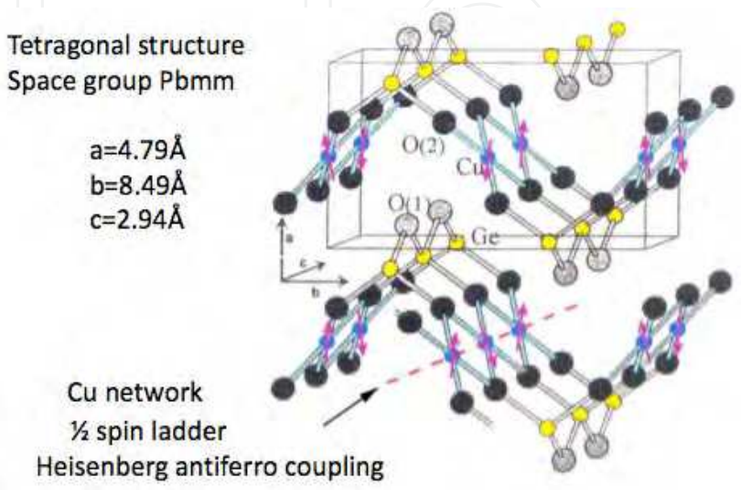
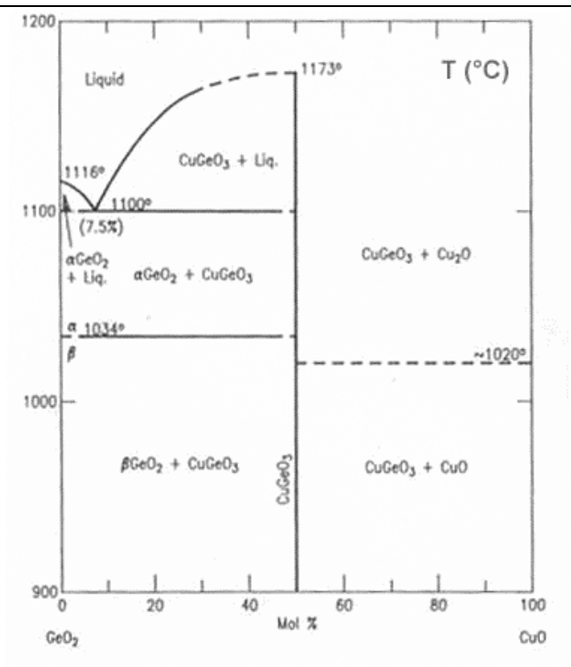


Fig. 2. $CuGeO_3$ crystallographic stacking.

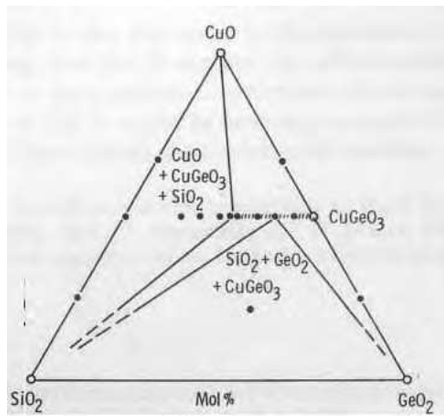
Phase diagram from Figure 3(a) shows that the cooling of $CuGeO_3$ from liquid phase is congruent. So, there is no phase separation in the pure compound. With silicon dioxide substitution a priori to GeO_2, the pseudo ternary diagram Figure 3(b) leads to expect that this property is conserved until 50% but our observations contradict this result. On the other hand, the phase diagram in Fig. 3 shows the existence of a multiphase domain limited by the single phase line $CuGe_{1-x}Si_xO_3$. The idea is thus to exploit this domain for inducing the second phase precipitation more strongly. The compositions of the starting material were $CuGe_xSi_yO_{1+2(x+y)}$ with x between 0.89 and 1.2 and for y between 0 and 0.3 and $1 \leq x+y \leq 1.4$, $0 \leq y/x \leq 0.33$ (see Figure 4). They break up from the liquid state into a monocrystalline matrix, incorporating some precipitates.

Crystal growth technique: The technique of crystalline growth known as 'floating zone method' (see Figure 1), that we used here, makes it possible to obtain monocrystals of a few cm long without stacking faults. By the way, the advantage of this technique is the possibility to grow high-purity single crystals since the melt has no contact with a crucible during the experiment. Homogeneous and dense feed rods were prepared using >99.99% pure powders of CuO, GeO_2 and SiO_2 as described in reference [7]. Required amounts of these powders were accurately weighted and mixed thoroughly. This mixture was then pressed into cylindrical rods of about 4mm in diameter and 8 cm in length under isostatic pressure of about 2500 bar. The feed rods, were then sintered in air at 1050°C for 24h. All composites (varying in the composition x and y) were grown from a pure $CuGeO_3$ monocrystalline seed aligned along its 'a' axis that defined the growth axis (see Figure 5). Growth was carried out with the 'a' axis of $CuGeO_3$ along the growth direction. The essential idea of this crystal growth technique is to establish a liquid zone between the single crystal seed and the polycrystalline feed rod. The vertical high-temperature gradients

required to stabilize the molten zone are ensured by focusing the image of two halogen lamps with two ellipsoidal mirrors. The molten zone temperature is precisely controlled by adjusting the lamp electric current magnitude. The crystal growth was carried out in an enclosed quartz tube where 2-atm oxygen pressure was established in order to prevent vaporization of CuO from the molten zone as much as possible. The growth rate (0.6 to 9 mm/h) is the rate at which the ensemble moves down from the furnace and this has a major influence on the characteristics of the grown crystal. The slow relative displacement of the heat source with respect to the liquid zone makes it possible to force the solidification of the fluid on the correctly directed monocrystal and thus the solidified material presents a continuous crystallographic character. This method yields single crystals of $Cu(Ge_{1-x}Si_x)O_3$ as well as two phase composite in the vicinity of the monocrystalline domain.



(a): $CuO\text{-}GeO_2$ binary phase diagram [12].



(b): Pseudo ternary diagram of $CuO\text{-}SiO_2\text{-}GeO_2$ at 600°C and 1kb. Lines are only indicative. [13]

Fig. 3. Phase diagrams for $CuGeO_3$.

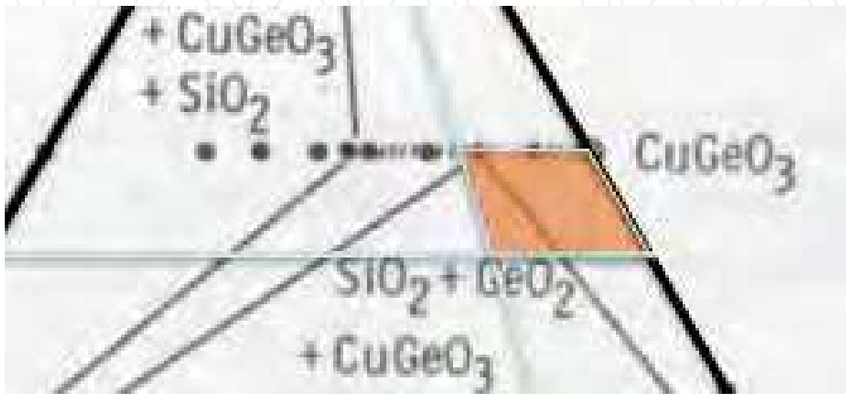


Fig. 4. Location of the compositions we have explored in the phase diagram of Figure 3

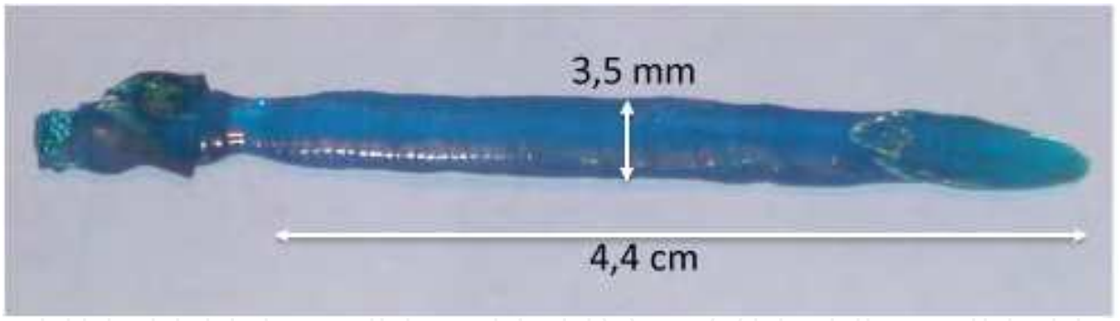


Fig. 5. Enlarged photograph showing the typical size of a crystal having the composition $CuGe_{0.915}Si_{0.085}O_3$. Growth rate 0.75-1.3 mm/h. 'a' axis is the growth axis. On the right hand, we can see the seed that defined the growth axis.

The growth rate has an important influence on the final structure of the crystal that evolves from the system. By carrying out the experiments at different rates, we conclude that, at this particular composition it is not possible to obtain ordered fibers if the rate exceeds 4 mm/h. However, there is a trade-off between the periodicity and the size and spacing of these fibers, as we increase the growth rate. Even though the size and spacing becomes smaller with increasing rate, it becomes more disordered. Therefore, we fixed this value at 1.3 mm/h and it was possible to obtain single crystals of about 14-cm long. The optimum growth rate varies with the composition, stoichiometry, etc. In this case also, an increase in the Si content beyond a limit (10%) results in more chaotic distribution of the fibers even if it is advantageous in obtaining smaller fiber diameter. It also restricts us in the range of feasible growth rates. Therefore, it is the compromise between the Si content and the growth rate that acts as the limitation to the minimum fiber size and spacing obtainable by this method. By working at slightly over stoichiometric composition, we are able to reduce this size up to 0.6 μm with spacing as small as 1.5 μm. What we observed was that, beyond a limit, the increase in Si will inhibit the ordered formation of silica fibers in the matrix.

3. Characterization

The crystals are deep blue in color (see Figure 6), translucent, and grow with an elliptical cross section, with the b and c axes of the structure being the minor (0.30 cm) and major (0.75 cm) axes of the ellipse, respectively. They can be easily cleaved along the (100) plane. Characterization of the samples was done by optical microscopy, SEM (secondary electrons and backscattered electrons), X-ray diffraction (XRD), EBSD (electrons backscattered diffraction), electron microprobe analysis, Raman micro-spectroscopy.

3.1 Optical microscopy and SEM

The obtained composites were cleaved and thin slices were observed by optical microscopy using polarized light. Precipitates are easily seen when they are larger than the micron. This indicates that the refraction index difference is large enough. Upon rotation of the sample about the 'a' axis, the brightness of the matrix varies whereas that of the rods does not change, indicating that the matrix is not isotropic but the rods are. The optical microscopy always showed two phases and not 3 for some composition as it is shown in Fig. 3b. It shows also the regularity of the precipitates, the heterogeneity of the distribution in some regions.



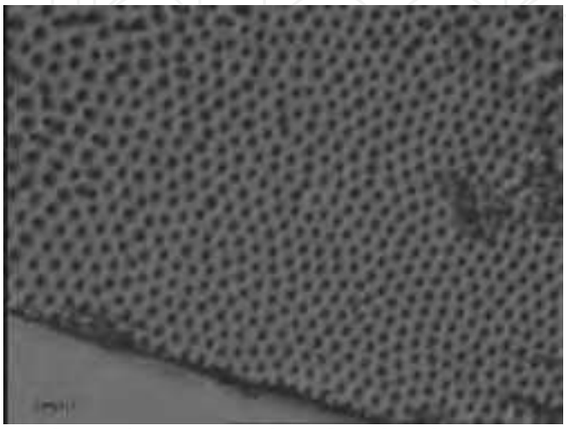
Fig. 6. Global view of a sample cleaved perpendicularly to its growth axis, the « a » axis. The sample composition was $CuGe_{0.915}Si_{0.085}O_3$ and it was grown at the rate 0.75-1.3 mm/h.

As we can see in Figure 6, the samples show concentric heterogeneities. There is a central region (brighter) containing precipitates. There is an external region clear from precipitates. There are regions with ordered precipitates of the same size e.g. the central region (appearing brighter in Fig. 6), and region rather disordered with various sizes and distances e.g. intermediate region. The outside part near the surface of the crystal never shows precipitates. Close to the borderline between intermediate region and external one, precipitates are aligned along equally spaced lines. The lines are more distant than in the central region.

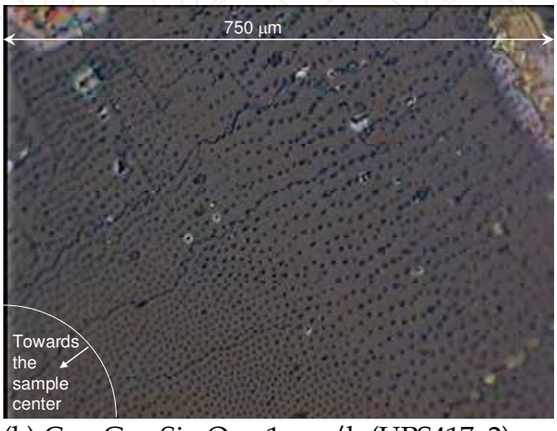
Figure 7 shows precipitates in the different region of the sample. In the central region, there is only a short range order. When moving to the outside, the precipitates` distribution varies. The distance and size increases. When reaching the surface, they disappear. In this region fibers are no more perpendicular but they are all tilted at the same angle. This is probably due to the curvature of the solid-liquid interface characteristic of the floating zone technique. Then, further from the center, the arrangement is more chaotic as we can see in Figure 7b. Figure 8 show the regularity of the precipitates in the central zone that is about 1 mm in diameter, in four of the numerous crystals that we elaborated. The smallest size and distance that we have obtained in the phase domain investigated is 0.6 and 1.4 μm respectively (see Figure 8d). Further observations by means of optical microscope in transmission and by successive cleaving perpendicular to 'a' axis showed that, in the central zone, these precipitates were long, columnar and perpendicular to the cleavage surface thus 'a' axis is along the crystal rods. They are therefore analogous to fibers.

One of the best ordered samples showing nearly periodically distributed fibers, was selected for the observation along a longitudinal section containing 'a' axis, to analyze whether these fibers run uniformly along the entire length of crystal without crossing over. A small-cleaved piece of sample was cut into two pieces. It was then fixed in epoxy resin and polished using SiC discs of grain sizes 600 and 1200 mesh for 10 minutes each and then using felt discs and diamond powder of granule sizes 6 μm, 3 μm, 1 μm and 0.25 μm

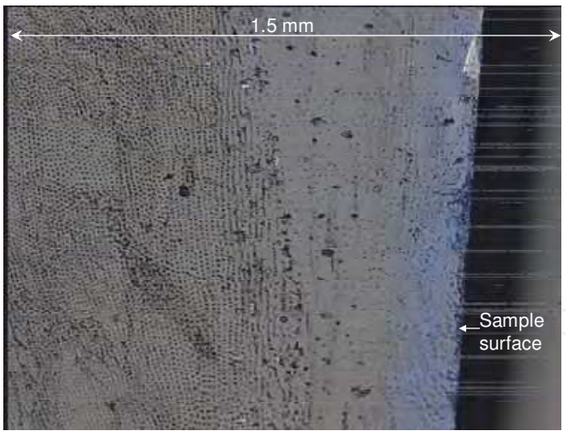
respectively for 10 minutes each. This was then observed using the optical microscope and the result is given in Figure 9. The photographs show that the fibers are quite uniform and grow along a great length of the crystal. It was observed that the length of the fiber as revealed from the photograph is almost 750 μm. The diameter ϕ of the fibers in this photograph from the sample with initial composition $CuGe_{0.915}Si_{0.085}O_3$ is around 4 μm and is more or less uniform throughout the length.



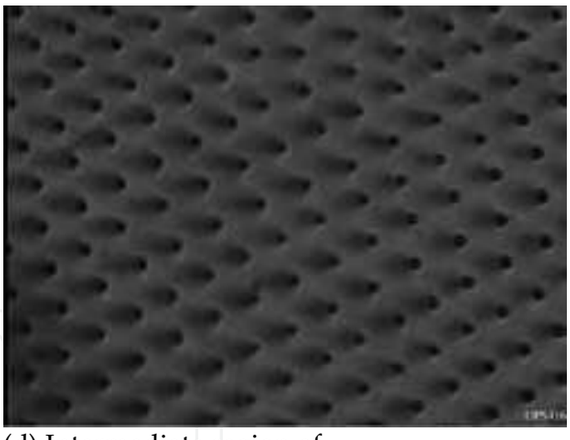
(a) Central region of $Cu_{1.0}Ge_{0.9}Si_{0.1}O_{3.0}$, 1mm/h (UPS417b) Precipitate distance is 4.1 microns, their size is 2.5 microns



(b) $Cu_{1.0}Ge_{0.9}Si_{0.1}O_{3.0}$, 1mm/h (UPS417a2)

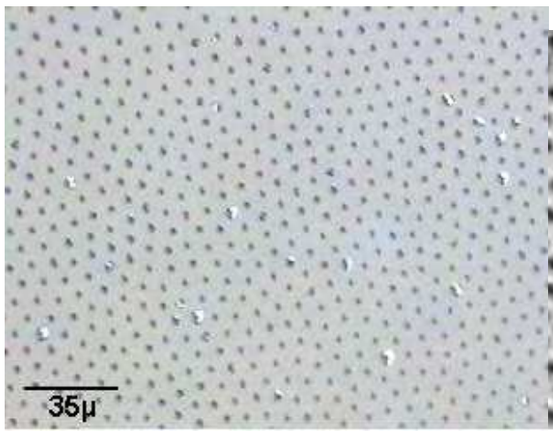


(c) $Cu_{1.000}Ge_{0.915}Si_{0.085}O_{3.000}$ (UPS416)

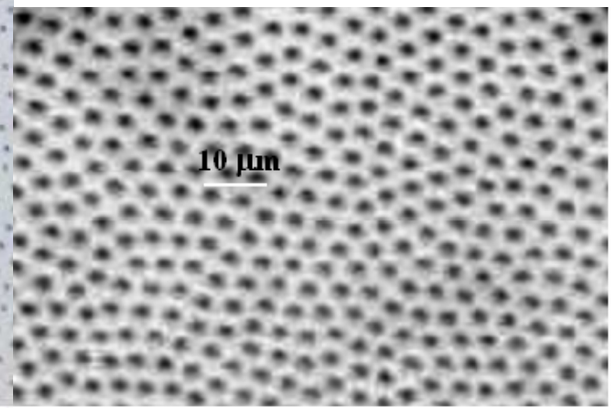


(d) Intermediate region of $Cu_{1.000}Ge_{0.915}Si_{0.085}O_{3.000}$ (UPS416) 0.75-1.3 mm/h, size 2.5 microns, distance 11.5 microns

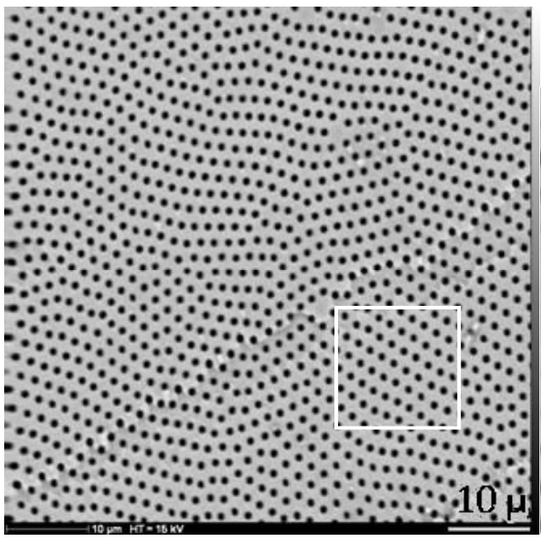
Fig. 7. Example of the structure of the samples: (a) typical image of the central region of the samples. Fibers are ordered on a short distance. (b) When moving out of the center, precipitate distance and size increase (c) when we are going closer to the surface the precipitates disappear. (d) In the intermediate region corresponding to c, the fibers appear tilted.



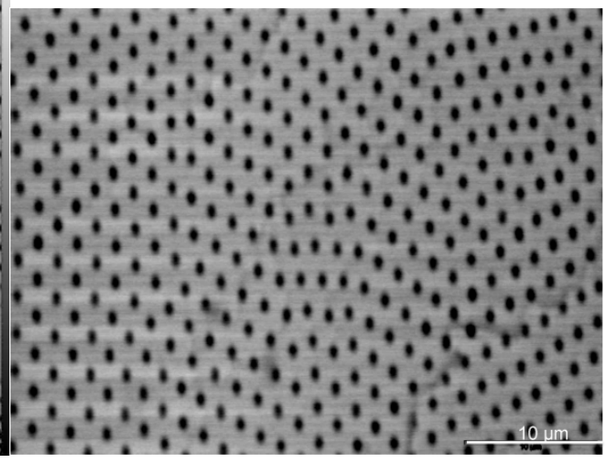
(a) Sample $Cu_{1.000}Ge_{0.915}Si_{0.085}O_{3.000}$ grown at 1 mm/h. The average distance between precipitates is 10 µm and the precipitate size is 4 µm.



(b) Sample with average distance between precipitates is 5 µm and the precipitate size is 3 µm.



(c) Sample $CuGe_{0.9}Si_{0.2}O_{3.2}$ grown at 2 mm/h (UPS430), fiber distance is 2.5±0,3 microns and diameter is 1.2±0,13 micron (filling factor 0.18).



(d) Sample $CuGe_{1,1}Si_{0.3}O_{3.8}$ grown at 2 mm/h (UPS436), fiber distance is 1.4±0,3 microns and diameter is 0.65±0,13 micron (filling factor 0.17).

Fig. 8. Variation of the central region of the samples when elaboration parameters are varied (SEM-backscattered electrons).

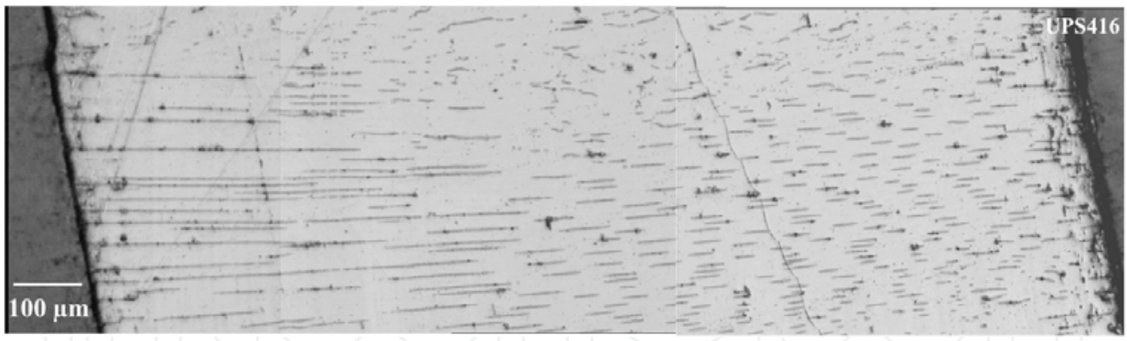


Fig. 9. Three images of the longitudinal section of the crystal were taken and carefully joined together to see the extension of the fibers running without distortion. The maximum length is around 750 microns and the fiber diameter is around 4 microns. Of course, as it is not possible to be exactly parallel to fiber axis, they are often cut during polishing. Sample $Cu_{0.20}Ge_{0.183}Si_{0.017}O_{0.60}$ (UPS416) growth rate 0.75-1.3 mm/h, fiber size 2.5µm, fiber distance 11.5 microns has been used here.

3.2 SEM-SE on tilted samples

Secondary electrons in SEM have a large field depth that is convenient for imaging on a large scale the surface of the sample that shows some topographies. However, it is necessary to tilt the sample sharply. Some images are displayed in Figure 10.

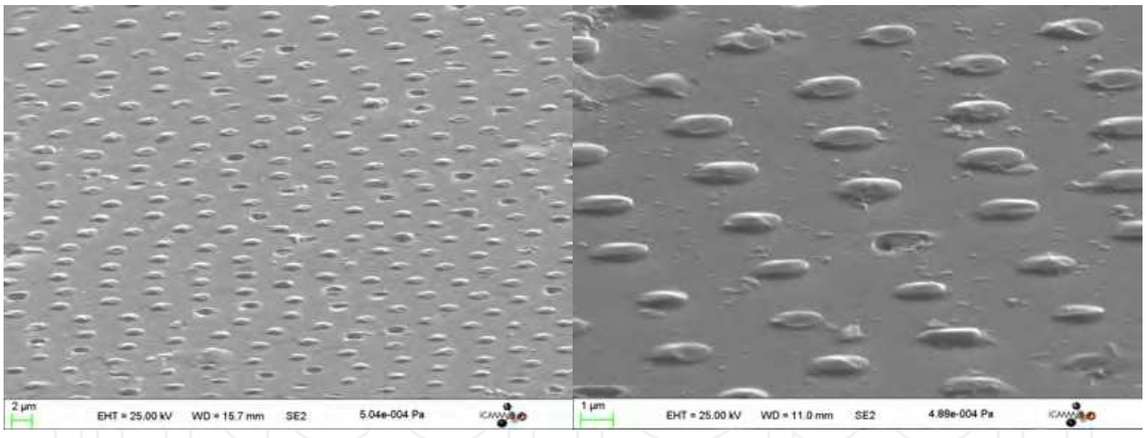


Fig. 10. Secondary electron image of the surface of a cleaved sample tilted under 70° upward. The fibers appearing here elliptic due to the tilt are actually circular.

As we can see, the fibers seem to protrude the surface of the sample. We checked using a phase shift interferometer whether it is actually the case. This observation can be made on both faces of the cleavage. Sometimes, fibers are broken below the surface level but commonly, they protrude. This means that a stress relaxation occurs and that they were in compression before cleaving. This can be due to smaller thermal expansion coefficient for the fiber than for the matrix.

In Fig. 11, the surface of the sample has not been perfectly cleaved and allows us to view the layer structure of the single crystal along an edge. It also reveals the channels where

the fibers were but in this case they disappeared during the cleaving. However, in the second image, a fiber remains showing that the crystallization around the fiber is not disturbed and the interface is very well defined. A transition region is not appearing. However, in Figure 12, we see better that a ring is appearing around the fiber compatible with a compression effect.

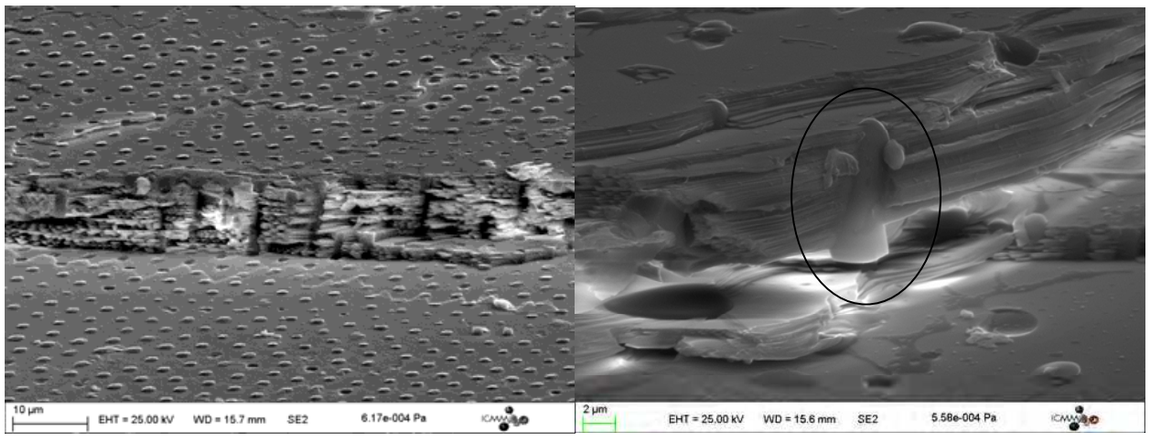


Fig. 11. Secondary electron image of surface of a sample not perfectly cleaved and tilted 70° upward. The ellipse in the photograph on the left shows a fiber end.

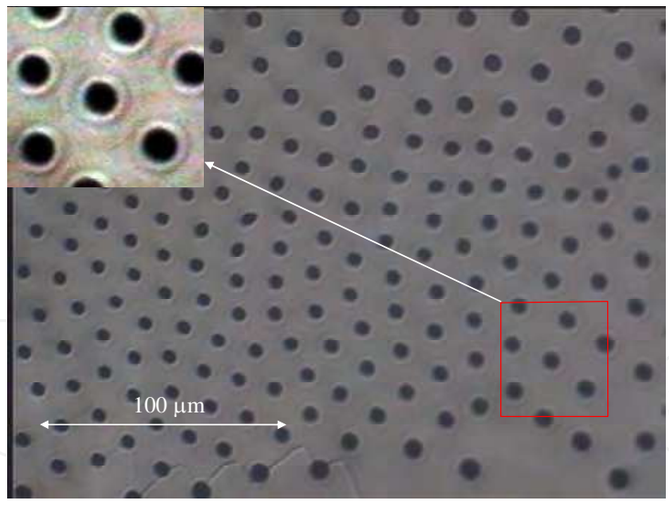


Fig. 12. This picture shows that around the fiber, a contrast is detected that seems to show a compression effect in agreement with the topography seen in SEM (sample UPS416).

3.3 X-ray diffraction

We have performed X-ray diffraction experiment (see fig.13) in order to identify additional lines among those of the well known cuprogermanate. Surprisingly, we detected the presence of only one crystalline phase, in contrast with the two phases observed by optical microscopy or SEM-EBS. This leads to think that the fibers are not crystallized.

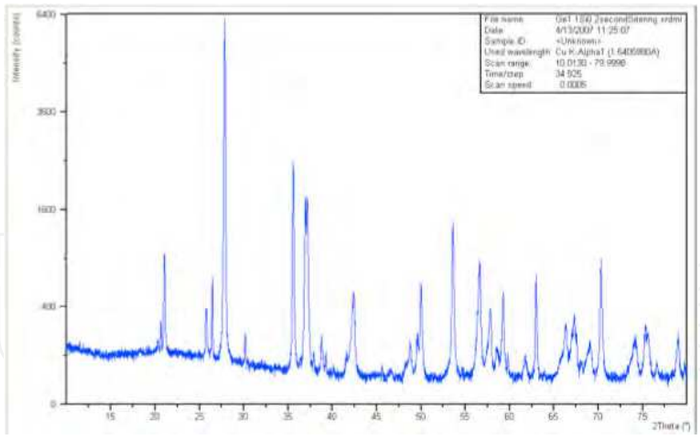


Fig. 13. X-ray diffraction pattern of a typical sample of $CuGe_xSi_yO_{1+2(x+y)}$. All the peaks in this spectrum can be labeled from $CuGeO_3$ space group.

3.4 SEM-EBSD (complementary observations, glass fibers are vitreous)

EBSD has been used to show that all fibers do not diffract the electron beam. The electron beam is incident on the sample under at an angle 70°. Electrons diffracted by crystal planes form Kossel cones. They are intercepted on a plane where they organized into lines called Kikuchi lines. Their indexation can lead to finding of crystal orientation if the space group and unit cell parameters are known. In our case, just the existence of diffraction is searched for. The resolution of the SEM-FEG used is good enough to analyze only one fiber. The accelerating voltage was 5kV and the working distance 10 mm. As we can see in Fig. 14 precipitates appear black. They do not diffract the backscattered electrons. We can thus conclude that the precipitates are vitreous.

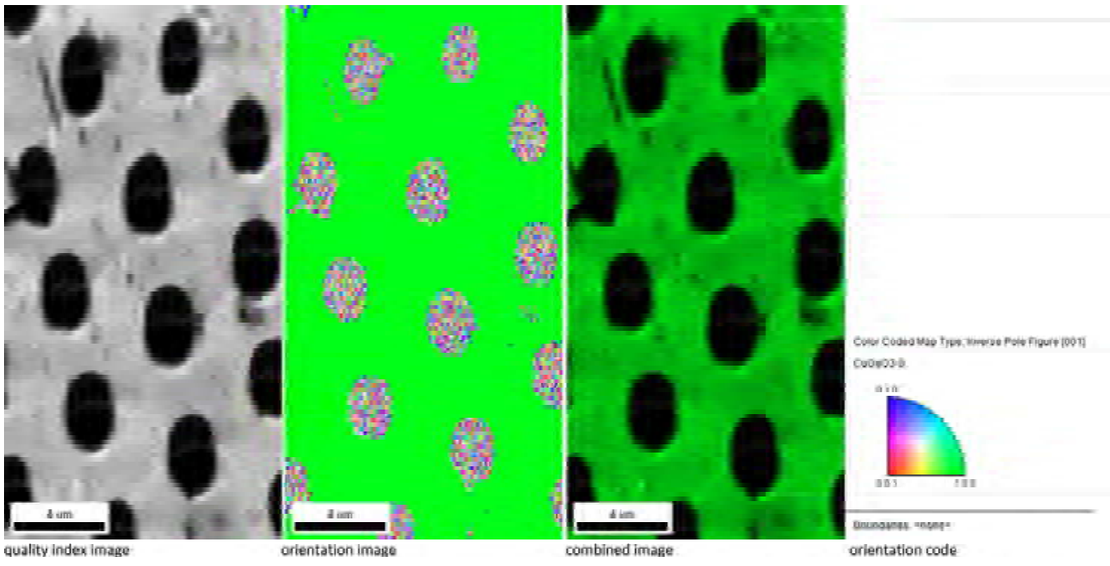


Fig. 14. Electron Backscattered Diffraction images. (a) EBSD image rebuilt from quality index of the Kikuchi diagrams (black = no diffraction). Precipitates appear actually black. The matrix has uniform brightness. (b) Orientation image, the matrix with uniform green color is a single crystal actually. (c) Combination of the two previous images.

3.5 Raman micro-spectroscopy analysis

Raman micro-spectroscopy can be used to identify a compound by its spectroscopic signature. It is based on the inelastic scattering of usually visible electromagnetic waves (energy exchange between the optical wave and the material vibration waves. Raman spectroscopy was performed in confocal mode with a pinhole of 300 microns and an objective of magnification 100x. The source of excitation was the 514 nm emission from an Ar^+ laser. To record the Raman spectra, the beam was focused on the surface of the material. Under these conditions, the lateral resolution is of the order of the micron whereas the depth resolution is about 30 microns. The acquisition time for the spectrum was fixed at 60s. By taking measurements between 200 and 4000 cm^{-1}, it was observed that, for our materials, Raman features were located only between 200 and 1500 cm^{-1}. The Raman spectra were recorded on the reference sample $CuGeO_3$ and on the sample doped with 10 % Si/(Si+Ge). Figure 15 shows the spectra collected between fibers and on a fiber. The spectrum of the

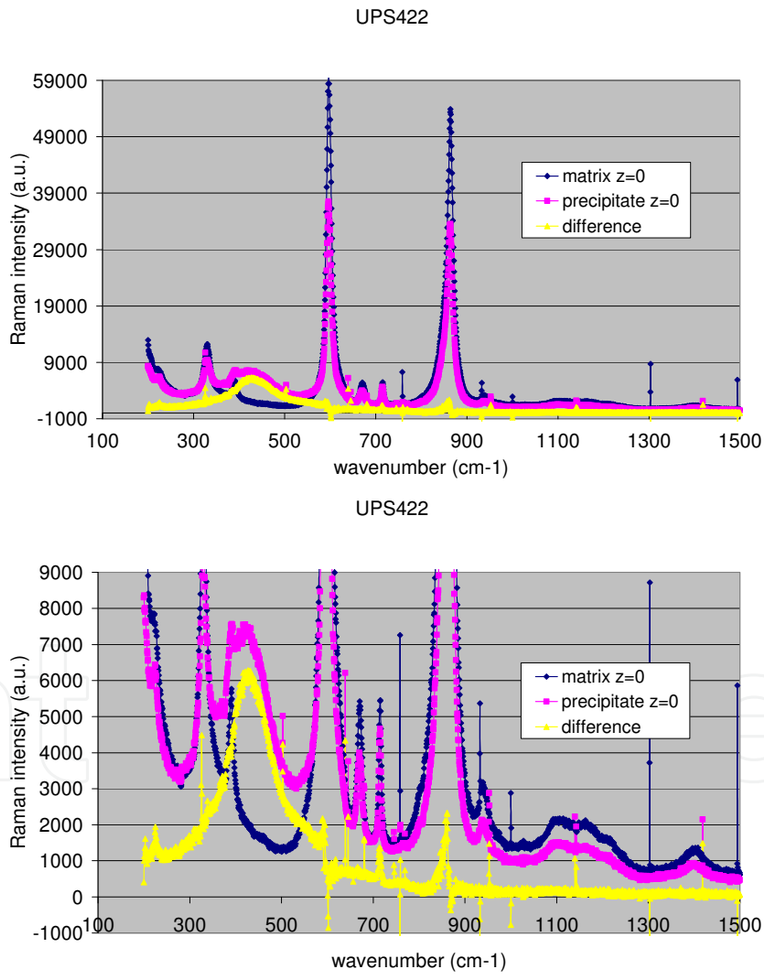


Fig. 15. Raman scattering spectra recorded at the surface of a cleaved sample with 10 % Si/(Si+Ge). One of the spectra has been recorded in the matrix surrounding the precipitate and the other one on the fiber itself. The third spectrum has been computed by weighted difference of the two others in order to eliminate the matrix spectrum as much as possible (UPS422). The second picture is an enhancement of the first one.

matrix, which is perfectly crystalline, is made of rather fine structures corresponding to the solid state vibration modes allowed in Raman scattering. Concerning the spectrum collected from the fiber region, even though the lateral resolution is larger than the fiber diameter, it can be seen however that it is identical to the spectrum of the matrix, except for an additional band around 430 cm^{-1}. To clearly express the difference between the two spectra, we performed a weighted difference between the spectrum of the precipitate and that of the matrix so as to eliminate, as much as possible, the lines from the matrix. One can thus clearly see the additional band in Figure 15, which has its maximum at 433 cm^{-1}. Its width is 107 cm^{-1}, which is significantly larger than the width of the crystal lines. It is thus possible to conclude that, in the fibers, there is no long-range order, in contrast to the crystals. Taking into account the results of the chemical analysis of the samples, it can be concluded that the fibers have a glass structure with an average composition intermediate between GeO_2 and SiO_2. We find the Raman spectra for this type of glass in the literature recently [14, 15], Raman spectra for SiO_2 and GeO_2 glasses are also well known. They present both a wide and intense band, respectively at 440 cm^{-1} and 416 cm^{-1}. Their respective widths are 234 cm^{-1} and 94 cm^{-1} [16]. The values that we measured are thus intermediate between these values in agreement with [15] and we can thus conclude from the Raman measurements that the probed precipitate is indeed vitreous.

3.6 Chemical composition by EPMA (it reveals that compensation occurs on the metal lattice)

In order to understand the phase separation, we performed chemical analyses. They were done by electron microprobe analysis (EPMA). Cu, Ge, Si and O, were analyzed independently. In this way, one could exclude measurements presenting a sum deviating from 100 wt %. A composition profiling was carried out in the zones containing precipitates. Monocrystal of $CuGeO_3$ and a silica blade were the references of measurement. Correct measurements were then converted into atomic percentage. The error bars were obtained by statistical average. For a global view of the content variations, we have recorded chemical profiles in dynamic mode. We can see large variations in Si and Cu profiles. It means that the profile is crossing a fiber. However, as we have no chance to cross exactly a fiber in the center, contrarily to static mode, the variation is never extremum. Of course, precise positioning has been achieved in the static mode. We made profiles on different samples with SiO_2 content from 8.5 to 30 mol %, only three measurements are shown below for demonstration.

3.6.1 In UPS 416, the nominal composition is $Cu(Ge_{0.915}, Si_{0.085})O_3 = Cu_{0.20}Ge_{0.183}Si_{0.017}O_{0.60}$

The external area, without precipitate, was measured separately in static mode, it showed the composition $Cu_{0.203}Ge_{0.191}Si_{0.014}O_{0.593}$. The ratio of the number of oxygen to metal (Cu, Ge, and Si) is a useful quantity for analyzing the differences in chemical composition at various regions. It is around 1.43 in this area instead of 1.5 in the perfect crystal. The external matter is thus slightly under-stoichiometric. One can also see, by comparing the chemical formula at this place with the nominal one, that it presents a loss in Si.

At the central area, the matter surrounding the fibers has the chemical composition: $Cu_{0.205}Ge_{0.197}Si_{0.015}O_{0.583}$ and here the ratio is 1.4. Thus this matter is also under-stoichiometric and again Si depressed (0.015 instead of 0.017). Under-stoichiometry undoubtedly corresponds to a natural reduction of Cu at high temperature during the elaboration process. The single crystal therefore should include oxygen vacancies.

The fibers show an average composition of $Cu_{0.05}Ge_{0.20}Si_{0.09}O_{0.66}$ with a ratio of oxygen to metal of 1.94. This is clearly a different chemical formula than the one for the matrix. This leads us to consider a formal composition of type MeO_2; like SiO_2 or GeO_2. In addition, we can also observe a clear enrichment of the net content in Si and a reduction in the quantity of Cu on comparison with the nominal composition. On the other hand, the sum of the oxygen quantities for saturating the metal content should yield 1.91 instead of 1.94. It can be thus considered that the compound is over-stoichiometric in oxygen. It should also be noted that the quantity of Si in the precipitates is higher than it can be obtained by a simple expulsion of CuO from the starting composition as can be seen by comparing the nominal composition rewritten in the form of $CuO+(Ge_{0.915}Si_{0.085})O_2$ with that of the precipitates $(Cu_{0.15}Ge_{0.61}Si_{0.27})O_2$. The chemical profile of Cu, Ge, Si and O made across the center (containing precipitates) and the surrounding area (clear from precipitate) is displayed in Fig. 16. It shows that O and Ge are almost constant along the profile. In contrast Si and Cu vary when a precipitate is crossed. We suspected a balance between only Si and Cu variation between the phases. The curve Cu+2Si actually confirms this observation. This curve does not show large variation anymore and suggests a valence charge balance between Cu and Si atoms.

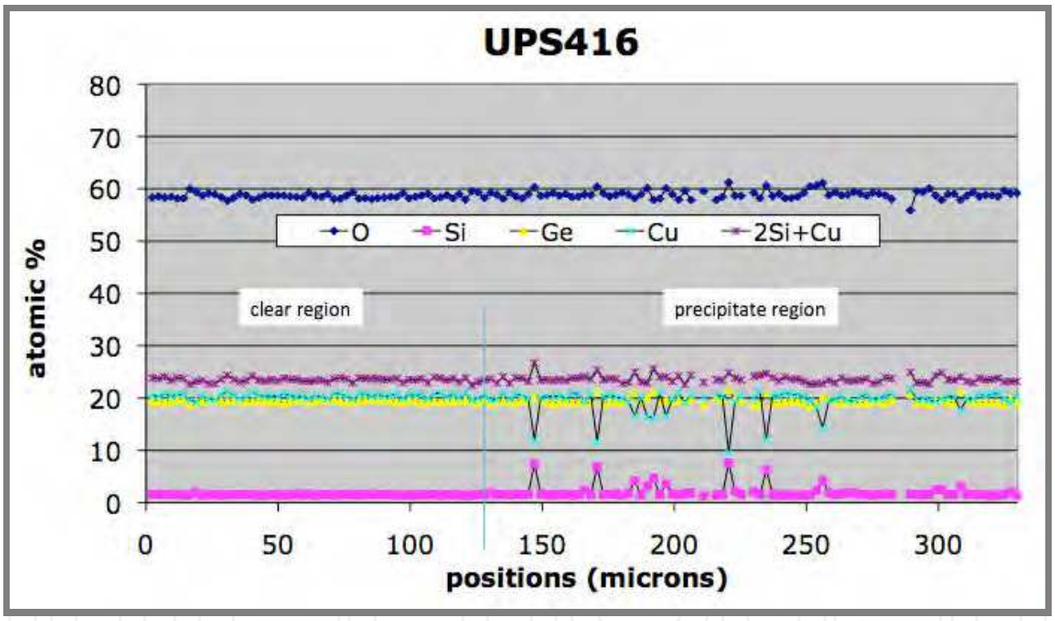


Fig. 16. Chemical profile of typical sample with the composition $Cu_{0.20}Ge_{0.183}Si_{0.017}O_{0.60}$. The region with precipitates is on the right hand side, the one without is on the left. Note the constancy of Ge atomic content from matrix and fibers. Note also the Cu variation, which is roughly the double of the Si one (Cu+2.Si curve).

3.6.2 In UPS 417, the nominal composition is $Cu(Ge_{0.900}, Si_{0.100})O_3$ $=Cu_{0.20}Ge_{0.180}Si_{0.020}O_{0.60}$

In this case also, several regions are analyzed (Fig. 17). The outermost region is without any precipitate and going towards the center; there is a region with disordered precipitates; a clear region and a small central region with ordered precipitates. The clear area exhibits a Si rich content with 2.5 to 3 at% and another area with a content poor in Si close to the biphased area. The average composition is $Cu_{0.189\pm0.007}Ge_{0.187\pm0.002}Si_{0.027\pm0.004}O_{0.597\pm0.004}$ with

oxygen to metal ration of 1.48. The other one shows the composition: $Cu_{0.206\pm0.005}Ge_{0.185\pm0.004}Si_{0.017\pm0.001}O_{0.592\pm0.006}$ with oxygen to metal ratio of 1.45. In the central region, the matrix composition is $Cu_{0.203}Ge_{0.187}Si_{0.018}O_{0.592}$. The precipitates have the following composition: $Cu_{0.055}Ge_{0.197}Si_{0.104}O_{0.644}$ with an oxygen-to-metal ratio of 1.91. We observe thus similar contrasts between matrix and precipitates similar to the previous sample.

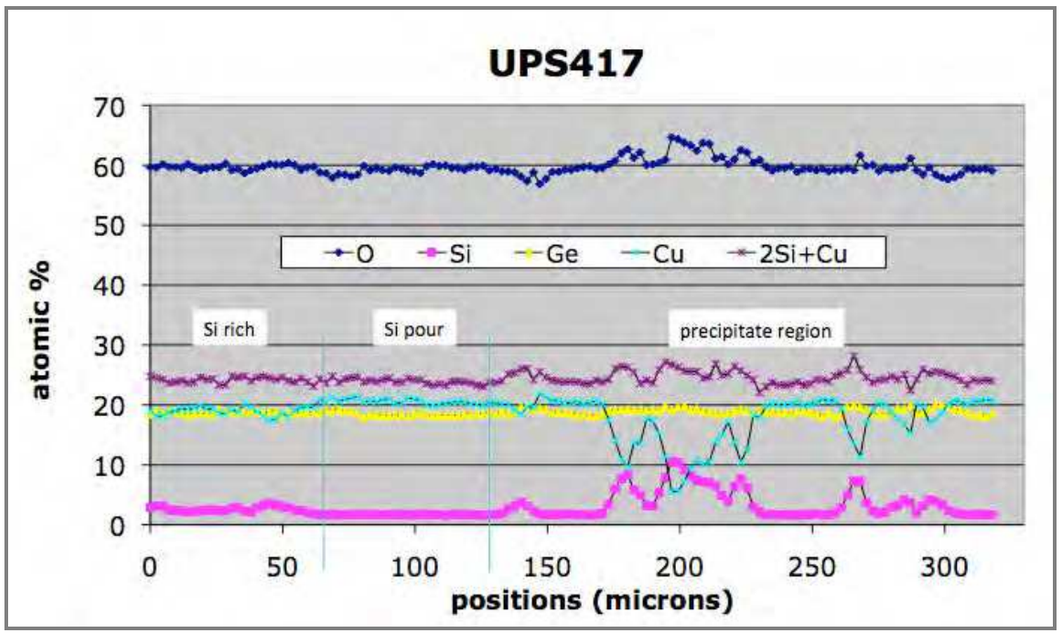


Fig. 17. Chemical profile of typical sample with the composition $Cu_{0.20}Ge_{0.180}Si_{0.020}O_{0.60}$. The region with precipitates is on the right hand side, the one without is on the left. Note the constancy of Ge atomic content from matrix and fibers. Note also the Cu variation, which is roughly the double of the Si one (Cu+2.Si curve).

3.6.3 In UPS 423, the nominal composition is $Cu(Ge_{0.800}, Si_{0.200})O_3$ $=Cu_{0.20}Ge_{0.160}Si_{0.040}O_{0.}60$. This sample contains precipitates but they are disordered

In the central region, the matrix appears with composition: $Cu_{0.210\pm0.005}Ge_{0.177\pm0.003}Si_{0.028\pm0.001}O_{0.580\pm0.004}$ with oxygen to metal ratio of 1.4 and with an depletion in Si compared to the nominal composition. The average composition of the precipitates is $Cu_{0.125\pm0.015}Ge_{0.160\pm0.004}Si_{0.11\pm0.01}O_{0.62\pm0.01}$ with oxygen to metal ratio of 1.57. Compared to the previous sample, here, the nominal composition contains more Si and therefore the precipitates contain more silicon too but the exchange is not in proportion. For starting compounds with 8.5 and 10% mol $SiO_2/(SiO_2+GeO_2)$, the fiber contains about 27% of Si/(Si+Ge+Cu), 59% of Ge/(Si+Ge+Cu) and 14% Cu/(Si+Ge+Cu). In this sample with 20% mol $SiO_2/(SiO_2+GeO_2)$ in the nominal compound, the fiber is made with 28% Si/(Si+Ge+Cu) and 41% Ge/(Si+Ge+Cu) but 31% Cu/(Si+Ge+Cu) i.e. more than twice the Cu content of the previous samples. Therefore, the oxygen to metal ratio does not reach 2 and even it is under-stoichiometric in oxygen. Nevertheless, the Ge content remains the same in all parts of the sample. However, the Cu/Si balance is now degraded (see Cu+2Si curve in Figure 18). What we observe also, is that the oxygen content does not show variation in proportion for balancing. We can suspect an electric charge of the fiber.

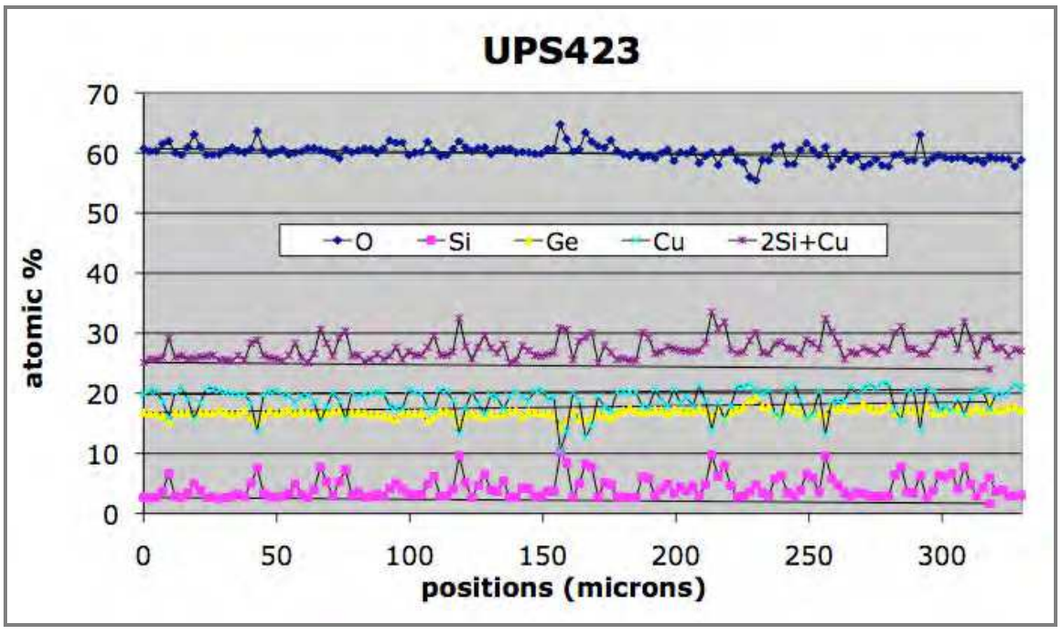


Fig. 18. Chemical profile of typical sample with the composition $Cu_{0.20}Ge_{0.160}Si_{0.040}O_{0.}60$. In this sample precipitates are everywhere across the profile. Note the constancy of Ge atomic content from matrix and fibers. Note also the Cu variation, which is roughly the double of the Si one (Cu+2Si curve).

3.6.4 Discussion and conclusions on the chemical observations

When precipitates are correctly ordered, we observed an over-stoichiometry in oxygen in fiber and an under-stoichiometry in the matrix. Although all the samples exhibit heterogeneities, the chemical composition of the cuprogermanate phase is rather homogeneous and close to the nominal one. Some small fluctuations in the Si content are nevertheless observed. They are compensated by Cu content variations.

For all the samples studied, which contain varying amounts of Si, we observed that the fibers are vitreous and have a $(Si+Ge)O_2$ type composition containing a small amount of CuO whereas the matrix has a composition close to the nominal one. We also observed that the fibers present a clear enrichment in Si in comparison with the surrounding matrix. More surprising is that this exchange does not disturb the Ge content. Quantitatively, the GeO_2 proportion is constant but the SiO_2 variation is 1/2 the one of CuO i.e. 2 CuO molecules in matrix structure is replaced by 1 molecules of SiO_2 in precipitate when they are ordered. We observe that the oxygen content increases consistently (we remind that oxygen content has been measured independently of the other constituents). The most external region is slightly silicon depressed when the central region is ordered. The constancy of Ge throughout the sample is remarkable. This is not the case for Si and Cu. Even more surprising is the balance between Cu and Si. There should be no constraint on oxygen diffusion in the liquid and so we expected no relation between Cu and Si. Therefore, the existence of such a relation means that oxygen migration is much lower than Cu and Si.

Now, one has to find an answer to three questions in order to master metamaterial elaboration: why is a second phase formed, why does it appear as micro rods (or fibers) and why are these rods regularly distributed?

For a ternary system like the one we used (CuO-SiO_2-GeO_2), when the starting composition falls into a 3-phase domain, the composition of the phases is defined by the intersection of a complex line (the connodal) with the domain boundaries. In this case, the molar proportion of each phase is defined by the position of the starting composition from each phase boundaries along the connodal, there is no free parameter. It is different with 2-phases case, the compositions of each phase depends on the starting composition. The phase molar proportion is defined by other constraint (not thermodynamically) e.g. the constancy of the Ge content whatever the phase.

In our case, we obtain a two phase composite with varying phase compositions when we change the starting composition. This is in principle, in agreement with the phase diagram of Breuer et al. [17]. However, the compositions of our phases are not the expected ones. We should obtain a combination of the $CuMeO_3$ phase and an almost pure GeO_2 phase. Instead, the fibers contain about 30% of Si, 40-60% of Ge and 15-30% Cu. We thus deduce that the formation of a vitreous phase allows germanosilicate glass to dissolve CuO and changes significantly the ternary CuO-SiO_2-GeO_2 phase diagram in which the two-phase domain is extended (see Figure 19).

The rod-type shape of the second phase and the regularity of the microstructure can then be explained as characteristic of a eutectic structure resulting from the decomposition, upon solidification, of a liquid into two solid phases. It is the right compromise between the thermodynamical energy and the surface energy. In such a eutectic transformation, taking place in a temperature gradient like the one available in the growth technique used in this study, the resulting aligned microstructures found are generally either lamellar or fibrous, depending on the volume fraction of the minor phase: when this fraction is smaller than about 30% the microstructure is rod-shaped, which is obviously the case here. Above 30% it is lamellar [18, 19]. The space period and also the size of the precipitates changes in the same samples and also the size but not continuously. There are region with precipitates of the same size and rather region rather disordered with various size and distance. When the size is constant, this means that the theory above is applicable.

The last question is why there is a spatially regular distribution? Some interpretation is given by Flemings [20] for eutectic solidification but can be applied more generally to our case. Decomposition of the liquid into two solid phases by eutectic reaction is limited by diffusion and reaction rate. This leads to a constrained control of the size and period of the minority phase distribution. In order to understand the relevant forces that lead to this situation, we tried a rationalization of our observations on a kinetics basis. We studied the differences in volume chemical content between the two solid phases (Table 1). Knowing the number of molecules per cm^{-3} of each phase ($CuMeO_3$ for the matter surrounding fibers and germania-silica glass for fibers themselves), we computed the changes per unit volume of each species in Table 1. The concentration of germanium and oxygen decreases only a little. This is apparently in contradiction with the atomic fraction (second column of Table 1) but change in atomic fraction does not mimic directly the change in the unit volume (third and above columns in Table 1) as we have to take into account the molecule volume. About the difference in Cu and Si, they appear complementary really in a ratio of 1 Si to 2 Cu. Therefore, we can conclude that during solidification of the liquid phase, there is an exchange of Cu and Si, on one hand, and a slight decrease in GeO_2 content in the fiber compared to the matrix.

Sample UPS417 $Cu_{0.20}Ge_{0.18}Si_{0.02}O_{0.60}$	Chemical formula (atomic %)	Number of atoms 10^{22} per cm^3				
		Cu	Ge	Si	O	Total
Matrix composition	$Cu_{0.203}Ge_{0.187}Si_{0.018}O_{0.592}$	1.70	1.56	0.15	4.94	8.35
Fiber composition	$Cu_{0.055}Ge_{0.197}Si_{0.104}O_{0.644}$	0.39	1.39	0.74	4.56	7.08
Difference (matrix to fiber)	$Cu_{-0.148}Ge_{0.010}Si_{0.086}O_{0.052}$	-1.31	- 0.15	0.594	- 0.33	-1.27

N.B.: There are 1.67 10^{22} molecules per cm^3 for $CuGeO_3$ crystal and 2.36 10^{22} molecules per cm^3 about for $1/3SiO_2+2/3GeO_2$ glass.

Table 1. Atomic content in each phase and their difference.

Sample UPS416 $Cu_{0.20}Ge_{0.183}Si_{0.017}O_{0.60}$	Chemical formula (atomic %)	Number of atoms 10^{22} per cm^3				
		Cu	Ge	Si	O	Total
Matrix composition	$Cu_{0.205}Ge_{0.197}Si_{0.015}O_{0.583}$	1.71	1.64	0.125	4.87	8.35
Fiber composition	$Cu_{0.05}Ge_{0.20}Si_{0.09}O_{0.66}$	0.354	1.43	0.637	4.67	7.08
Difference (matrix to fiber)	$Cu_{-0.148}Ge_{0.010}Si_{0.086}O_{0.052}$	-1.35	- 0.21	0.61	- 0.20	-1.27

N.B.: There are 1.67 1022 molecules per cm3 for CuGeO3 crystal and 2.36 1022 molecules per cm3 about for 1/3SiO2+2/3GeO2 glass.

Table 2. Atomic content in each phase and their difference.

We can now arise the question on the transformation of the system under cooling in the phase diagram. As a matter of fact, the observation of a first phase with composition $CuMeO_3$ where Me is a mixture between Ge, Si, and a second phase with composition $Me'O_2$ where Me' is also a metallic mixture, means that the starting liquid did not keep the composition of the rod in particular, $CuMeO_3$ in the case considered in the table. Unfortunately, it was not possible to know the composition of the liquid phase, but we can deduce it by calculation. In this direction, considering the sample with 8.5% at Si, from the optical and SEM observations, we know the filling factor in the central region in 2D is 16%. With this information, and considering that there is invariance along the growth axis, we can achieve the calculation by combining the chemical formula of one phase with the other one. This is done in the Table 3.

Table 3 shows for the central region of the sample that the Ge or Si content have not changed whereas Cu and O show a similar decrease. It is thus clear that the liquid has been losing CuO under heating. We can remind here that from chemical analysis, we found that the external region without precipitates is SiO_2 depressed. As the GeO_2 content remains almost constant, and because a flux of SiO_2 is compensated by a flux of CuO, it yields that CuO migrated from the center to the surface and SiO_2 migrated in the reverse direction. This is likely due to thermal gradient. Therefore, for this specific composition, this migration moved the system (corresponding to the ordered region) from the congruent line to the two phase domain as we show in Figure 18.

Sample UPS416 $Cu_{0.20}Ge_{0.183}Si_{0.017}O_{0.60}$	Chemical formula (atomic %)	Number of atoms 10^{22} per cm^3				
		Cu	Ge	Si	O	Total
Matrix filling factor=0.84		1.71	1.64	0.125	4.87	8.34
Fiber filling factor=0.16		0.354	1.43	0.637	4.67	7.08
Average composition in $at.cm^{-3}$ i.e. estimate for the liquid phase		1.49	1.60	0.207	4.84	8.14
Nominal composition in $at.cm^{-3}$ i.e. composition of the ceramics rod		1.67	1.53	0.14	5.01	8.35
Difference average minus nominal		-0.18	0.07	0.07	-0.17	-0.21

Table 3. Computation of the liquid phase composition.



Fig. 19. Ternary diagram for $CuO\text{-}SiO_2\text{-}GeO_2$ from [13] (1kb, 600°C) on which we have placed the estimated composition for the liquid phase (red point), the matrix composition (open blue circle) and the fiber composition (solid blue circle). Dashed blue lines are re-estimate of the location of the phase boundaries. The green point is the starting composition for samples $Cu_{0.20}Ge_{0.18}Si_{0.02}O_{0.60}$

Figure 18 shows the location of the previous example in the phase diagram. As we can see, the rod composition in green moved to the red point on losing CuO, and then under cooling, the two phase composition is defined by the line linking the two blue points and the matter conservation. On one hand, the matrix composition surrounding the fiber is defined by the congruent line. On the other hand, since the fibers contain CuO, this means that a phase boundary (dashed blue line) is missing in the diagram. Below this line, there exists a silica glass containing CuO. In addition, we can say, that between the two blue points, it is not a three phases domain but a two phases one. Finally, as we had seen that the liquid phase corresponding to ordered area, moved to glass boundary, we made further experiments with increasing content in glass formers. This gave then results with the smallest size and distances between fibers (See Figure 8d).

In order to obtain spacing between fibers compatible with the second telecom window (1.5 µm), we studied several parameters of growth. For a fixed filling factor *f*: $d^2R=a$, $\pi\phi^2/4d^2=f$,

$\phi^2 R = b$ where d is the fiber distance, R is the growth rate, ϕ is the fiber diameter. f is dependent of the phase diagram. 'a' and 'b' are constants depending on several thermodynamic and kinetic quantities themselves depending on nominal chemical composition and temperature, R can be considered as a free parameter [20]. Experimentally, we proved that the distance between fibers could be reduced at least down to 1.4 μm and fiber diameter to about 0.6 μm keeping a rather good order. Good fiber ordering is obtained for filling factor lying between 0.126 and 0.140. Below this range, the order may be good enough but the fiber distance is quite large. Above that, the ordering degrades. Since the filling factor is partly defined by the nominal composition, the increase in silicon content leads to an increase in the filling factor but it may lead also to disordering.

There is so a series of conditions for obtaining good ordering. This ensemble of conditions suggests an instability like the Turing one [21]. As a matter of fact, we can remark that at the beginning there is too much MO_2 in the liquid to elaborate a single crystal (this is deduced from phase diagram). This induced Si content fluctuations achieved by diffusion. As Si content increased in some places, at these places the structure stabilized into silica-germania glass increasing the driving force for Si to increase its concentration (since it is known that SiO_2 adopts vitreous state easily). *In other words, MO_2 formation is self-catalyzed.* On the other hand, copper is hardly soluble in this phase from which it is expelled. This increases the copper concentration out of fibers and creates new $CuMeO_3$ molecules that can dissolve more Si. This inhibits thus the Si diffusion and the MO_2 formation. So, *we find in this scheme the ingredients for Turing instability: a species self-catalyzed (MO_2) and inhibited by another one (CuO*). These are necessary conditions but not sufficient, Si should diffuse more slowly than Cu. There is no diffusion measurement available in $CuGeO_3$ (contrarily to $(Si,Ge)O_2$). Nevertheless, it is known that Cu diffuses much faster than Si in vitreous matter [22, 23]. We thus think that ordered fiber distribution in our case is a self-organization relevant from Turing structures.

4. Optical properties

Figure 20 is a comparison of Fourier transforms of the two samples shown in Figure 8. We observe a circle around the central point in Figure 19(a) with a non-zero thickness whereas there are just a few points in Figure 20(b). This corresponds to isotropy of equally distant point distribution in Figure 8(b) whereas (c) is well ordered at the first and subsequent neighbors. If sample in Figure 20(b) is recognized as a **metacrystal**, sample in Figure 20(a) exhibits properties of a glass with a rather well defined first neighbor coordination shell but an isotropy due to random long range order. We can thus call this structure **metaglass**.

From Fourier transforms (FT), we can extract several structural quantities:

- The size of the central point yields coherence length, it is 50 μm horizontally and 33 μm vertically for sample (a). This means 4.3 to 6.0 fiber periods, whereas for sample (b), it is 11.5 μm which corresponds to 5.5-7.7 fiber periods.
- The distance from the first point (Figure 20(b)) or circle (Figure 19(a)) to the center point yields the fiber distance by simple inversion. It is 7.7 μm vertically and 8.3 μm horizontally for sample (a) whereas it is 2.1 μm and 1.5 μm respectively for sample (b). For sample (a), the dispersion of the first neighbor distance is around 20%.
- In FT image of sample (a) image, we can see a larger intensity at the higher and lower bounds of the circle. This means that a texture begins to appear in this sample. We

have elaborated other samples with a texture more developed, intermediate between FT of sample (a) and sample (b). Diffraction directions appear in that case as spots on a circle.

The next point is to observe that only one circle (sample (a)) or one series of points located on an ellipse (sample (b)) is detected. This arises from the ratio of the fiber size to the period or the filling factor. Due to the large value of this ratio (0.43), the FT domain is strongly limited to the first points around the central spot. This can be good for application as the intensity is concentrated only in several directions [24].

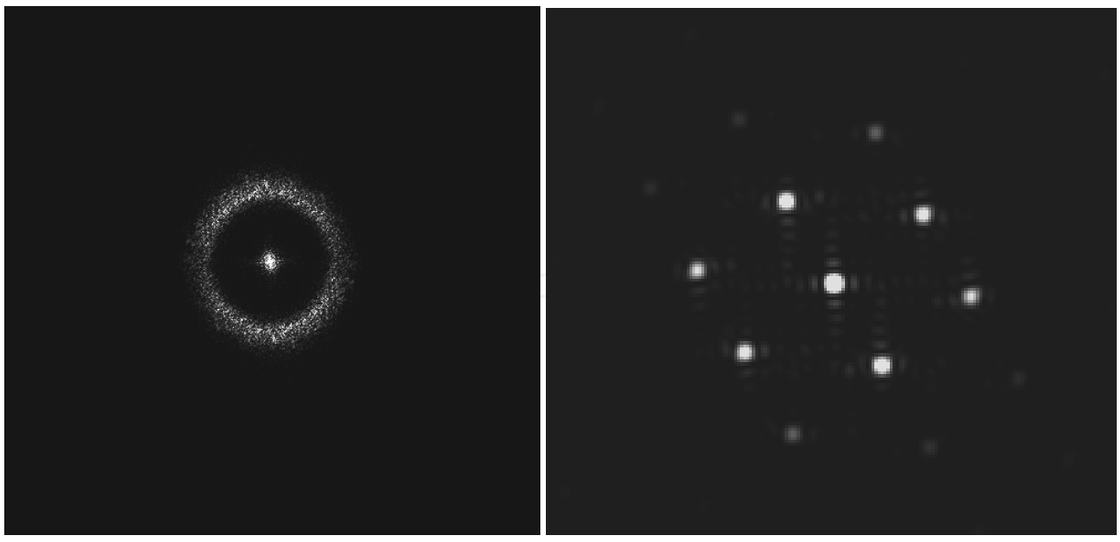
A thin slice of the sample was cleaved along the (100) plane or perpendicular to the 'a' axis, for observation under optical microscope. This can be done both in reflection and transmission modes using either natural or polarized white light. The precipitates are highlighted easily with respect to their monocrystalline surroundings, because of sufficiently high contrast in refractive index (the difference is about 0.32, matrix index=1.77 (average value), fiber index 1.45). The samples are not homogeneous in the conditions we used as it can be seen from the difference in color in the center and on the outer regions of the sample surface (see Fig. 2). These regions are concentric, indicated by a lighter shade of blue at the center and a darker one outward. The use of polarized light indicates that the matrix is not isotropic. 'b' and 'c' are the neutral crystal axes perpendicular to 'a' axis (unfortunately we were not able to measure this birefringence). On the contrary, the precipitates do not provide any contrast, which means that they have an isotropic structure in the cleavage plane.

5. Towards Photonic Crystals (PC) working in the IR

Optical microscopy of the sample shows regular arrangement of a large number of silica fibers. Therefore, it was selected for further chemical treatment to develop a material with characteristics close to that of a PC. The essential idea is to etch out the fibers from the crystalline matrix, using HF acid, and thus obtain a higher refractive index difference between the two dielectric phases. To begin with, a piece of pure $CuGeO_3$ was HF treated for 30 min, in 40% HF acid, to make sure that the crystal is not etched away significantly. It is because the aim is to remove the fibers from the sample, without affecting its monocrystalline surroundings. There is no observable difference in the structure of the material before and after the procedure. A thin-cleaved slice of the sample (of thickness 0.5mm) was taken for the experiment. It was immersed in 20% HF acid for 30 min and was observed under the optical microscope (Figure 21a and 21b). There is significant difference in the structure of the sample after the procedure. Apparently, the surface of the material has been cleaned and the etched sample reveals lamellar structures around the fibers. Also the circular cross section of the fiber changes to a rhomboid shape after etching. This sample was again immersed in acid and the microscope images are given in Figure 22a and 22b. The purpose was to confirm, whether the fibers are completely etched off the sample. Figure 21a is the image after 1 h and Figure 22b is taken after keeping it in acid for a longer time. The image of the crystal in Figure 22b shows some white dots at the center of the periodic structures, which were the locations of fibers in the non-etched sample. This means that the fiber from that region has been etched off across the entire thickness of the sample. We further confirmed this by the surface topography from a phase shift interferometer and also by the AFM studies, which we do not include in this article since it carries no more

information than those we already showed in the SEM and optical microscope images. However, to ensure that the fibers are indeed etched away completely, we did a layman experiment, placing it over a colored transparent slide to observe the image under optical microscope, in the transmission mode. The results were positive, but it is to be mentioned that the thickness of the sample was only less than 0.5mm. We measured the etching rate of the sample by comparing its thickness with a reference, after repeated etching procedure. It is about 12 μm/h.

SEM analysis: The SEM images of this sample using the backscattered (BSE) and secondary electron (SE) modes are given in Figure 23a and b, respectively. The BSE results give an indication of the chemical differences at various locations, whereas the SE measurements are more related to the topography of the material. One interesting feature that we observed is the change in the shape of the cross sectional area occupied by the fibers. The fibers themselves had circular cross section. However, after their removal a location assumes a rhomboid shape. One might be lead thinking that there is a preferential direction along which the etching took place faster, which is the direction of the minor axis of the crystal. Even if the reasons are not clear, we propose two hypotheses. (1) It is the surface tension of the fibers while in liquid form that enabled them to assume circular cross section. When the fibers are removed, the tension releases, and the surrounding matrix takes the shape decided by its crystalline properties. (2) On the border of the fibers the crystalline matrix is also etched away slightly, and the rhomboid shape is an indication of the crystallographic axis in the growth direction [25]. It can also be seen that the appearance of the white lines and the variations in the color of the surrounding matrix are perfectly repetitive. We further confirmed using phase shift interferometer technique and AFM that these correspond to variation in the depth profile.



(a) Fourier transform associated to Figure 8b. The radius of the first circle is 0,125 μm^{-1} in average.

(b) Fourier transform associated to the region delimited by white square in Figure 8c. The distance of the neighbouring central point is 0.58 μm^{-1} in average.

Fig. 20. Fourier Transforms from pictures in Figure 8.

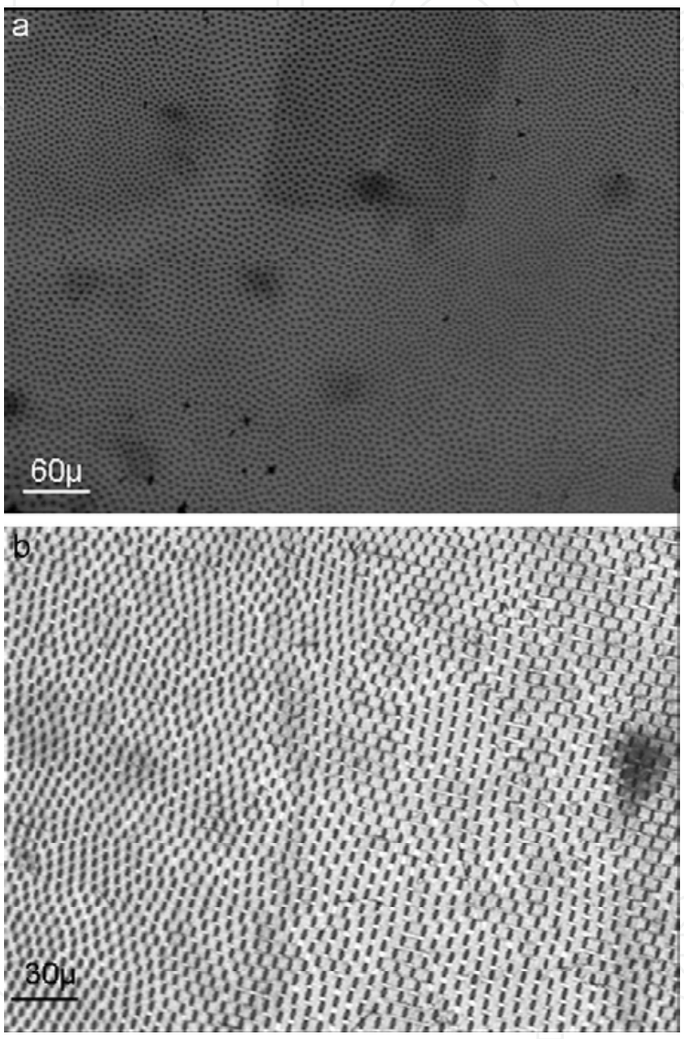


Fig. 21. Photograph of the sample before (a) and after (b) HF treatment for 30 min in 20% acid. There are obvious differences in the structure of the crystalline matrix after the procedure.

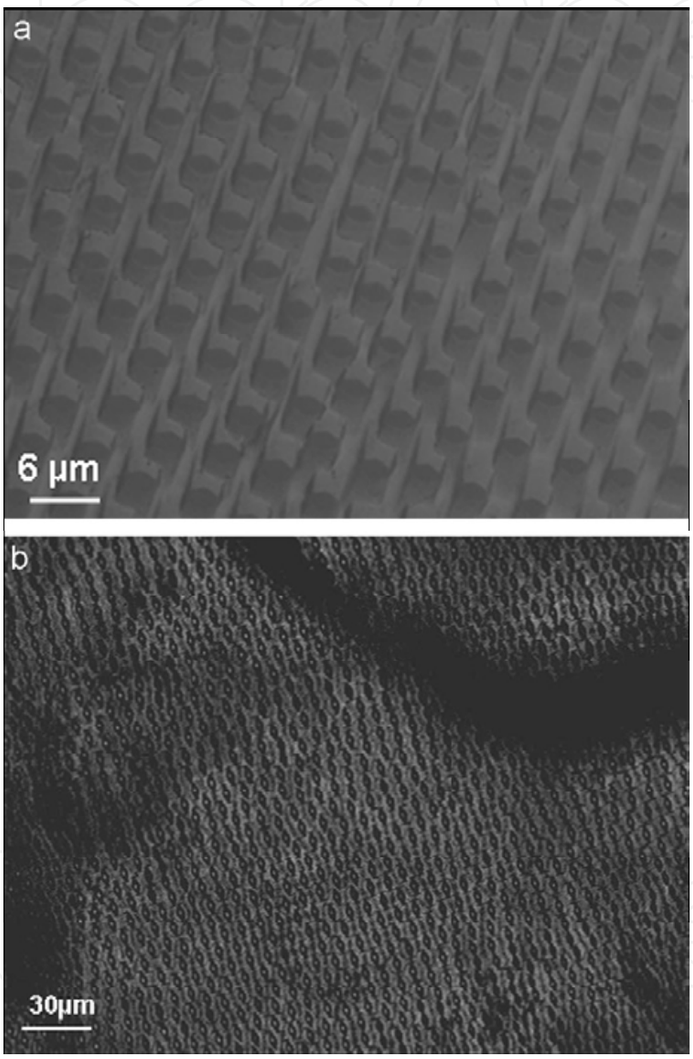


Fig. 22. Photograph of the sample after HF treatment for 3 h (a) at high magnification and (b) shows the picture after keeping the sample in acid for a longer time such that the fibers are etched off. This is indicated by the appearance of white dots.

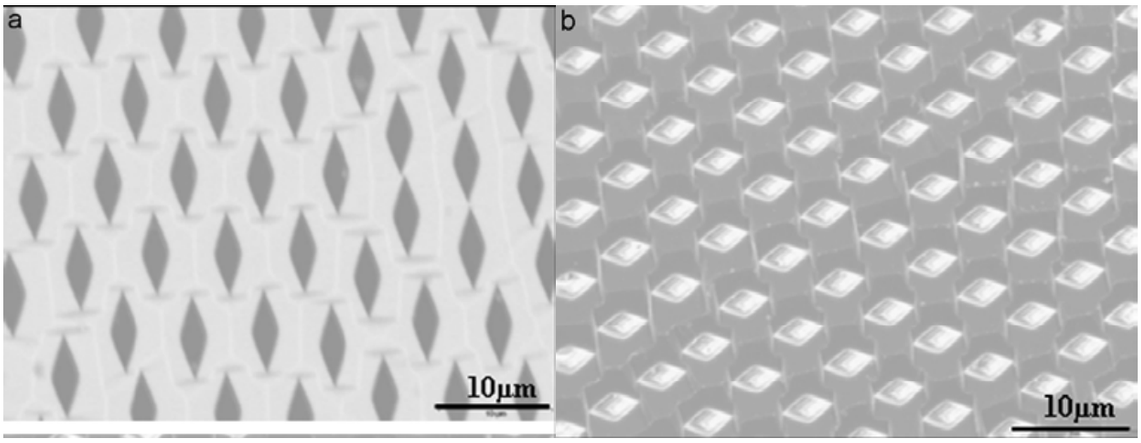


Fig. 23. A thin-cleaved slice of the sample (ofthickness0.5mm) was taken for the experiment. It was immersed in 20% HF acid for 30 min and was observed Under the Optical microscope. There is significant difference in the structure of the sample after the procedure. Apparently, the surface of the material has been cleaned and the etched sample reveals lamellar structures around the fibers. Also the circular cross section of the fiber changes to a rhomboid shape after etching.

6. Conclusion

We synthesized from the melt an aligned two-phase material whose minority phase is vitreous and the majority one, crystalline through self-organization. This is original, as far as we know. Another example of glass precipitation (Si_3N_4) in a crystalline matrix (Fe) has been published [26] but no order appears at all. The samples that we have synthesized are monocrystals of $CuMeO_3$ type (with Me = Ge or Si) with orthorhombic crystalline structure containing germania-silica glass fibers $(Ge_{0,7}Si_{0,3})O_2$. The fibers can have sub-micrometer size, regularly spaced, close to a compact hexagonal stacking with a period slightly above the micron. This regular microstructure was obtained only for certain ranges of Si content and growth rate.

Furthermore, the manipulation of the parameters controlling the microstructure of composite presented above (diameter and distribution of fibers) and the beginning of rationalization in the frame of Turing structure, opens up ways for finding other systems exhibiting similar structures. This will be valuable for a better control of the degree of ordering and for finding chemical systems with much lower light absorption in the telecom window. In the present composition, the absorption coefficient is around 2 cm^{-1}, quite flat for wavelength ranging from 1 to 4 µm.

These two dielectric structures react differently to HF acid, which we exploit to remove the fibers from the matrix without affecting the crystal. So far this has been successful until a length limit of 0.5mm. There are research results indicating that photonic band gaps can also be observed in quasi-periodic dielectric structures [16, 27]. Some researchers have already reported that PCs show complete band gaps, if the dielectric contrast is sufficiently high [28, 29]. We used the finite difference time domain method for photonic band gap (PBG) calculation assuming a hexagonal lattice. Even if the results are not conclusive, what we can say at this stage is that, before etching there was no indication of a band gap; however, after

improving the refractive index difference from 0.32 to 0.77, we observed that a PBG opened up in the TE mode (but not in the TM mode).
The next question, here, is the use of such a composite. We have to firstly underline that we have fabricated real 2D ordered composite as the translation symmetry along the thickness is much larger than the material period in the perpendicular plane. Thus, vertically, the intensity remains concentrated without any diffraction. One application is wavelength extraction: with sample with optimal order, it is possible to diffract light at 1.5 μm under an angle of 50° and to collect 1 nm wide channel for injection in a 10 μm wide waveguide 3cm away from the center of the crystal. With a crystal with short coherence length, it is not necessary to turn the crystal for fulfilling a Bragg condition and thus a star demultiplexing is achievable. But this is quite modest application with the system we used here. We think possible that our metamaterials could be useful for bio-optical applications. We are optimistic to reach metamaterial applications in the visible and maybe photonic crystal ones by investigating other composites achievable by the same method.

7. Acknowledgements

This work has been performed with a postdoctoral support of the University of Paris Sud 11. The authors are deeply grateful to Prof. Revcolevschi for his great scientific help on this subject.

8. References

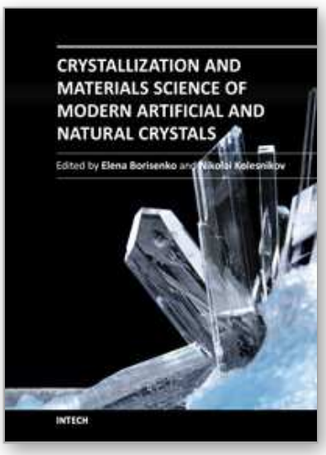
[1] C. N. R. Rao, A. Müller, and A. K. Cheetham, *The chemistry of Nanomaterials, Synthesis, properties and applications.* (Wiley-VCH, 2004), Vol. 1-2.
[2] C. M. Soukoulis, S. Linden, and M. Wegener, "Metamaterials are designed to have structures that provide optical properties not found in nature. If their capacity can be extended, new kinds of devices for imaging and control of light will be possible.," Science 315., 47-49 (2007).
[3] J. B. Pendry, "Negative Refraction Makes a Perfect Lens," Physical Review Letters 85, 3966-3969 (2000).
[4] A. Starr, P. Rye, D. Smith, and S. Nemat-Nasser, "Fabrication and characterization of a negative-refractive-index composite metamaterial," Physical Review B 70, 113102 (2004).
[5] P. N. Prasad, *Nanophotonics* (John Wiley and sons, 2004).
[6] M. Bassi, P. Camagni, R. Rolli, G. Samoggia, F. Parmigiani, G. Dhalenne, and A. Revcolevschi, "Optical absorption of CuGeO3," Physical Review B 54, 11030-11033 (1996).
[7] G. Dhalenne, A. Revcolevschi, J. C. Rouchaud, and M. Federoff, "Floating zone crystal growth of pure and Si or Zn substituted copper germanate $CuGeO_3$.," Material Research Bulletin 32, 939-946 (1997).
[8] J. P. Pouget, L. P. Regnault, M. Ain, B. Hennion, J. P. Renard, P. Veillet, G. Dhalenne, and A. Revcolevschi, "Structural evidence for a spin peierls gound state in the quasi-one dimensional compound $CuGeO_3$.," Physical Review B 72, 4037-4040 (1994).
[9] A. Revcolevschi, "Nickel oxide – based aligned eutectics," in *Tailoring Multiphase and Composite Ceramics.*, R. E. M. Tressler, G L; Pantano, C G; Newnham, R E, ed. (Plenum publishing corporetion, Pennsylvania, USA, 1986).

[10] A. Revcolevschi and G. Dhalenne, "Engineering Oxide-Oxide and Metal-Oxide microstructures in directionally solidified eutectics.," Advanced Materials 5, 657-662 (1993).
[11] A. Revcolevschi, G. Dhalenne, and D. Michel, "Interfaces in directionally solidified oxide-oxide eutectics.," Material Science Forum 29, 173-198 (1988).
[12] E. I. Speranskaya, Inorganic Materials 3, 1271-1277 (1967).
[13] U. Müller and E. Conradi, "Fehlordnung bei Verbindungen MX_3 mit Schichtenstruktur.," Zeitschrift für Kristallographie 176, 233-261 (1986).
[14] G. S. Henderson, D. R. Neuville, B. Cochain, and L. Cormier, "The structure of GeO2-SiO2 glasses and melts: A Raman spectroscopy study," Journal of Non-Crystalline Solids 355, 468-474 (2009).
[15] O. Majérus, L. Cormier, J. P. Itié, L. Galoisy, D. Neuville, and G. Calas, "Pressure-induced Ge coordination change and polyamorphism in SiO2-GeO2 glasses," Journal of Non-Crystalline Solids 345, 34-38 (2004).
[16] F. L. Galeener, "The Raman spectra of defects in neutron bombarded and Ge-rich vitreous GeO_2.," J. of Non-Crystalline Solids 40, 527-533 (1980).
[17] K. H. Breuer, W. Eysel, and M. Behruzi, "Copper (II) silicates and germanates with chain structures II. Crystal chemistry*," Zeitschrift für Kristallographie 176, 219-232 (1986).
[18] K. Jackson and J. Hunt, "Lamellar and rod eutectic growth," AIME MET SOC TRANS 236, 1129-1142 (1966).
[19] W. Kurz and D. J. Fisher, "Fundamentals of solidification," Trans Tech Publications Ltd, Trans Tech House, 4711, Aedermannsdorf, Switzerland, 1986. 244 (1986).
[20] M. C. Flemings, *Flemings (1974) Solidification processing* (McGraw-Hill (New York), 1974).
[21] A. M. Turing, "The chemical basis of morphogenesis," Philosophical Transactions of the Royal Society of London. Series B, Biological Sciences 237, 37 (1952).
[22] J. D. McBrayer, R. Swanson, and T. Sigmon, "Diffusion of metals in silicon dioxide," Journal of the Electrochemical Society 133, 1242 (1986).
[23] H. A. Schaeffer, "Diffusion-controlled processes in glass forming melts.," J. of Non-Crystalline Solids. 67, 19-33 (1984).
[24] I. L. Gheorma, S. Haas, and A. Levi, "Aperiodic nanophotonic design," Journal of applied physics 95, 1420 (2004).
[25] D. A. Pawlak, K. Kolodziejak, S. Turczynski, J. Kisielewski, K. Rozniatowski, R. Diduszko, M. Kaczkan, and M. Malinowski, "Self-organized, rodlike, micrometer-scale microstructure of Tb3Sc2Al3O12-TbScO3: Pr eutectic," Chemistry of materials 18, 2450-2457 (2006).
[26] E. Mittemeijer, M. Biglari, A. Boettger, N. Pers, W. Sloof, and F. Tichelaar, "Amorphous precipitates in a crystalline matrix; Precipitation of amorphous Si {sub 3} N {sub 4} in {alpha}-Fe," Scripta materialia 41(1999).
[27] H. Gersen, T. Karle, R. Engelen, W. Bogaerts, J. Korterik, N. Van Hulst, T. Krauss, and L. Kuipers, "Direct observation of Bloch harmonics and negative phase velocity in photonic crystal waveguides," Physical review letters 94, 123901 (2005).
[28] S. G. Johnson and J. D. Joannopoulos, "Three-dimensionally periodic dielectric layered structure with omnidirectional photonic band gap," Applied Physics Letters 77, 3490-3492 (2000).

[29] J. H. Park, W. S. Choi, H. Y. Koo, J. C. Hong, and D. Y. Kim, "Doped colloidal photonic crystal structure with refractive index chirping to the 111 crystallographic axis," Langmuir 22, 94-100 (2006).

IntechOpen

IntechOpen



Crystallization and Materials Science of Modern Artificial and Natural Crystals

Edited by Dr. Elena Borisenko

ISBN 978-953-307-608-9
Hard cover, 328 pages
Publisher InTech
Published online 20, January, 2012
Published in print edition January, 2012

Crystal growth is an important process, which forms the basis for a wide variety of natural phenomena and engineering developments. This book provides a unique opportunity for a reader to gain knowledge about various aspects of crystal growth from advanced inorganic materials to inorganic/organic composites, it unravels some problems of molecular crystallizations and shows advances in growth of pharmaceutical crystals, it tells about biomineralization of mollusks and cryoprotection of living cells, it gives a chance to learn about statistics of chiral asymmetry in crystal structure.

How to reference

In order to correctly reference this scholarly work, feel free to copy and paste the following:

Bertrand Poumellec, Matthieu Lancry, Santhi Ani-Joseph, Guy Dhalenne and Romuald Saint Martin (2012). Elaboration of a Specific Class of Metamaterial: Glass in Single Crystal, Crystallization and Materials Science of Modern Artificial and Natural Crystals, Dr. Elena Borisenko (Ed.), ISBN: 978-953-307-608-9, InTech, Available from: http://www.intechopen.com/books/crystallization-and-materials-science-of-modern-artificial-and-natural-crystals/elaboration-of-a-speciic-class-of-metamaterials-glass-in-single-crystal-

INTECH
open science | open minds

InTech Europe
University Campus STeP Ri
Slavka Krautzeka 83/A
51000 Rijeka, Croatia
Phone: +385 (51) 770 447
Fax: +385 (51) 686 166
www.intechopen.com

InTech China
Unit 405, Office Block, Hotel Equatorial Shanghai
No.65, Yan An Road (West), Shanghai, 200040, China
中国上海市延安西路65号上海国际贵都大饭店办公楼405单元
Phone: +86-21-62489820
Fax: +86-21-62489821

© 2012 The Author(s). Licensee IntechOpen. This is an open access article distributed under the terms of the Creative Commons Attribution 3.0 License, which permits unrestricted use, distribution, and reproduction in any medium, provided the original work is properly cited.

IntechOpen

IntechOpen